ARTICLE

Detailed Description of Pulse Isotopic Exchange Method for Analyzing Oxygen Surface Exchange Behavior on Oxide Ion Conductors

Chun-lin Song[a*], Jian-xin Yi[b], Yan Yan[a*]

a. School of Materials and Energy, Southwest University, Chongqing 400715, China
b. State Key Laboratory of Fire Science, Department of Safety Science and Engineering, University of Science and Technology of China, Hefei 230026, China

(Dated: Received on November 5, 2018; Accepted on February 17, 2019)

A novel pulse ^{18}O-^{16}O isotopic exchange (PIE) technique for measurement of the rate of oxygen surface exchange of oxide ion conductors was presented. The technique employs a continuous flow packed-bed micro-reactor loaded with the oxide powder. The isothermal response to an ^{18}O-enriched pulse passing through the reactor, thereby maintaining chemical equilibrium, is measured by on-line mass spectrometry. Evaluation of the apparent exchange rate follows from the uptake of ^{18}O by the oxide at given reactor residence time and surface area available for exchange. The developed PIE technique is rapid, simple and highly suitable for screening and systematic studies. No rapid heating/quenching steps are required to facilitate ^{18}O tracer anneal or analysis, as in other commonly used techniques based upon oxygen isotopic exchange. Moreover, the relative distribution of the oxygen isotopologues $^{18}O_2$, $^{16}O^{18}O$, and $^{16}O_2$ in the effluent pulse provides insight into the mechanism of the oxygen exchange reaction. The PIE technique has been demonstrated by measuring the exchange rate of selected oxides with enhanced oxide ionic conductivity in the range of 350−900 °C. Analysis of the experimental data in terms of a model with two consecutive, lumped steps for the isotopic exchange reaction shows that for mixed conductors $Ba_{0.5}Sr_{0.5}Co_{0.8}Fe_{0.2}O_{3-\delta}$ (BSCF) and $La_2NiO_{4+\delta}$ the reaction is limited by the apparent rate of dissociative adsorption of O_2 molecules at the oxide surface. For yttria-stabilized zirconia (YSZ), a change-over takes place, from rate-limitations by oxygen incorporation below ∼800 °C to rate-limitations by O_2 dissociative adsorption above this temperature. Good agreement is obtained with exchange rates reported for these materials in literature.

Key words: Isotopic exchange, Oxygen surface exchange, Ion conductor, $Ba_{0.5}Sr_{0.5}Co_{0.8}Fe_{0.2}O_{3-\delta}$

I. INTRODUCTION

The increasing energy demand and cost, in conjunction with the growing public awareness of the need for energy production with minimal environmental impact, has generated significant research endeavors over the past two decades towards development of oxygen transport membranes and solid oxide fuel cells (SOFCs) [1−7]. Both devices incorporate solid oxide electrolytes and/or oxides with highly mobile oxide ions and electronic charge carriers, so-called mixed conductors. Their performance strongly relies on fast oxygen exchange at relevant gas/solid interfaces, shown in FIG. 1. Since the rate may govern the overall transport kinetics, detailed knowledge of the oxygen surface exchange reaction is a pre-requisite for further development of these devices.

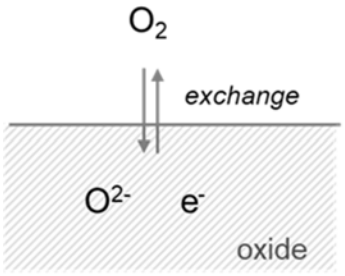

FIG. 1 Reversible oxygen exchange between the gas phase and the oxide.

A variety of methods have been used to probe the surface exchange kinetics on oxide surfaces, such as electrical conductivity relaxation (ECR) [8−11], oxygen permeation [12], ^{18}O-^{16}O isotopic exchange [13−20], electrochemical impedance spectroscopy (EIS) [21, 22], oxygen partial pressure relaxation [23], and pulse isotopic exchange (PIE) [24]. Especially, methods based upon isotope exchange are considered useful for obtaining in-

*Authors to whom correspondence should be addressed. E-mail: chunlinsong@swu.edu.cn, yanyan2013@swu.edu.cn

formation on surface oxygen exchange. There are, in essence, two different approaches, which are based upon ^{18}O isotope analysis of either the oxide bulk or the gas phase. In the former, referred to as isotope exchange depth-profiling (IEDP), a dense sample is subjected to an ^{18}O-^{16}O exchange anneal, followed by *ex situ* depth profiling of the ^{18}O tracer diffusion profile by ion beam analysis, such as secondary ion mass spectrometry (SIMS) [20] or nuclear reaction analysis (NRA) [25]. The experiments enable simultaneous determination of the oxygen diffusion coefficient (D^*) and surface exchange coefficient (k^*), which are obtained by fitting the concentration depth profile to the appropriate solution of the diffusion equation. In the second technique, referred to as isotopic exchange gas-phase equilibration (IEGE), the equilibration of the oxygen isotope fractions in the gas phase during the ^{18}O-^{16}O exchange anneal is *in situ* monitored as a function of time using mass spectrometry [21, 26, 27]. Both techniques have their intrinsic advantages and disadvantages. The advantage of the gas phase technique over the depth-profiling technique is that the exchange rate information is obtained on the mechanism of the surface exchange reaction. The latter may be evaluated from the time-dependence of the concentration of oxygen isotopologues, $^{18}O_2$, $^{16}O^{18}O$, and $^{16}O_2$, formed by isotopic scrambling and recombination of oxygen adatoms at the oxide surface. Both techniques, however, involve a number of rapid heating, pre- and/or diffusion annealing, and quenching steps. Not only is this time consuming, but also it needs great care in order to avoid introduction of artefacts and errors into the assessment of the kinetic parameters [28, 29].

In this work, we introduce a novel technique, referred to as pulse-response ^{18}O-^{16}O isotopic exchange (PIE). The technique allows rapid assessment of the oxygen surface exchange rates of solid oxide ion conductors at chosen conditions of temperature and oxygen partial pressure. The PIE technique is demonstrated by measuring the oxygen surface exchange rate of yttria-stabilized zirconia (YSZ), $Ba_{0.5}Sr_{0.5}Co_{0.8}Fe_{0.2}O_{3-\delta}$ (BSCF), and $La_2NiO_{4+\delta}$. YSZ is widely used as oxide solid electrolyte, while the mixed ionic-electronic conductors oxides BSCF and $La_2NiO_{4+\delta}$ have potential for application either as cathode material for the intermediate-temperature SOFC or as oxygen transport membrane [4, 8]. Different from IEDP and IEGE, no rapid heating and/or quenching steps are required in application of the PIE technique. Since the technique relies on gas phase analysis of the concentrations of $^{18}O_2$, $^{16}O^{18}O$, and $^{16}O_2$, kinetic information of the oxygen surface exchange reaction can be extracted from the experimental data.

II. THEORY

A. Principle of pulse isotopic exchange

The pulse isotopic exchange (PIE) technique developed in this work employs a packed-bed micro-reactor loaded with the oxide powder. After equilibration of the oxide at chosen oxygen partial pressure and temperature, the response to an ^{18}O-enriched pulse fed through the reactor operating under continuous flow conditions is measured. The principle of the measurement is shown schematically in FIG. 2.

The overall surface exchange rate is calculated from the mean residence time, the total surface area of the oxide powder available for exchange, and the uptake of ^{18}O by the oxide. The latter is evaluated from the known ^{18}O tracer concentration in the injected pulse, and that in the effluent pulse measured by on-line mass spectrometry at the exit of the reactor. After passage of the pulse, the conditions may be changed and the oxide sample equilibrates for another pulse experiment. The PIE technique enables fast acquisition of the surface exchange rate of the oxide under investigation as a function of environmental parameters, *e.g.*, temperature and oxygen partial pressure.

PIE differs from steady-state isotopic transient kinetic analysis technique (SSITKA) frequently used in studies of heterogeneous catalysis [30]. SSITKA involves isothermal switching the isotopic composition of the feed stream flowing through the packed bed reactor. For evaluation of the oxygen exchange rate, numerical modelling is required to analyze the kinetic data as a function of time-on-stream [31]. The boundary conditions associated with PIE make evaluation of the surface exchange rate rather simple and straight forward. The mode of gas transport in PIE further differs from that in conventional pulse and TAP (temporal analysis of products) micro-reactors where either an inert gas, such as helium or nitrogen, is used as carrier gas, or the exit of the reactor is exposed to high vacuum conditions [32].

The mathematical analysis of the data of PIE is rather simple. Consider a differential volume element traversing through the reactor. Under the assumption of (i) ideal plug flow behaviour, (ii) homogeneous packing of the oxide in the reactor, and (iii) relative to surface exchange, fast lattice diffusion of oxygen, *i.e.*, a large diffusion length of ^{18}O in the (non-porous) oxide, mass balance analysis yields the first order linear differential equation:

$$n_r \frac{\partial f_g^{18}}{\partial t} = -\Re_0 S_r \left(f_g^{18} - f_o^{18}\right) \tag{1}$$

where $\Re_0$ (in mol $O{\cdot}m^{-2}{\cdot}s^{-1}$) is the surface exchange rate, n_r is the number of moles of oxygen atoms in free volume of packed bed reactor (which is twice the number of O_2 molecules), and S_r is the surface area of the oxide for the entire packed bed reactor. f_g^{18} and f_o^{18} are the ^{18}O isotope fractions in the gas phase and oxide, respectively. It is noted that f_g^{18} is calculated from the molar fractions of $^{16}O^{18}O$ and $^{18}O_2$ in the gas phase: $f_g^{18}=f_g^{36}+0.5f_g^{34}$.

The ^{18}O fraction in the gas phase is much higher

DOI:10.1063/1674-0068/cjcp1811245

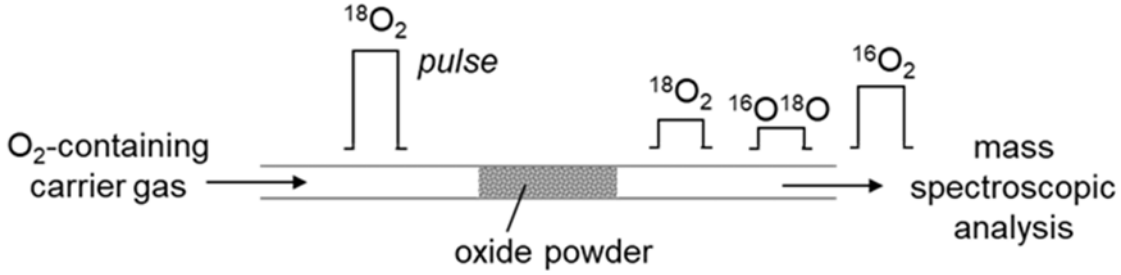

FIG. 2 Principle scheme of the pulse ^{18}O-^{16}O isotope exchange technique.

than that in the oxide. In the absence of significant accumulation of ^{18}O in the oxide or at the oxide surface, *i.e*, assuming $f_{\rm o}^{18}\approx 0$, it follows

$$n_{\rm r}\frac{\partial f_{\rm g}^{18}}{\partial t} = -\Re_0 S_{\rm r} f_{\rm g}^{18} \tag{2}$$

Splitting of the variables and integration over a time yield

$$f_{\rm g,o}^{18}(t) = f_{\rm g,i}^{18}\cdot\exp\left(-\frac{\Re_0 S_{\rm r} t}{n_{\rm r}}\right) \tag{3}$$

which for, $t=\tau_{\rm r}$, where $\tau_{\rm r}$ is the residence time of the reactor, can be re-written as

$$\Re_0 = -\frac{n_{\rm r}}{\tau_{\rm r} S}\ln\left(\frac{f_{\rm g,o}^{18}}{f_{\rm g,i}^{18}}\right) \tag{4}$$

In Eqs. (3) and (4), $f_{\rm g,i}^{18}$ and $f_{\rm g,o}^{18}$ denote the ^{18}O isotope fractions in the gas phase at the inlet and outlet of the reactor, respectively. The validity of these equations extends to any finite number of ^{18}O atoms in the pulse volume as long as the boundary conditions adopted during their derivation are satisfied. The residence time (or space time) of the reactor can be calculated from

$$\tau_{\rm r} = \frac{V_{\rm r}\varepsilon}{F} \tag{5}$$

where $V_{\rm r}$ is the total volume of the packed bed reactor, ε is the bed void fraction, and F is the volumetric flow rate of the gas at chosen temperature. With the aid of Eq.(5), Eq.(4) can be written in more practical forms, as

$$\begin{aligned}\Re_0 &= -\frac{c_{\rm g}F}{S}\ln\left(\frac{f_{\rm g,o}^{18}}{f_{\rm g,i}^{18}}\right)\\ &= -\frac{F_{\rm m}}{S}\ln\left(\frac{f_{\rm g,o}^{18}}{f_{\rm g,i}^{18}}\right)\end{aligned} \tag{6}$$

where $c_{\rm g}=n_{\rm r}/\varepsilon V_{\rm r}$ is the oxygen concentration in the gas phase, and $F_{\rm m}=Fc_g$ (in mol O·s^{-1}) is the molar flow rate, or using the ideal gas law, in the form $c_{\rm g}=2p{\rm O}_2/RT$, as

$$\Re_0 = -\frac{2p{\rm O}_2}{RS}\cdot\frac{F}{T}\ln\left(\frac{f_{\rm g,o}^{18}}{f_{\rm g,i}^{18}}\right) \tag{7}$$

The factor 2 in this equation arises from the fact that the oxygen atoms in the gas phase are present as O_2 molecules. The flow rate F_0 at temperature T_0 (usually room temperature) can be converted to the audit flow rate F at temperature T, using $F=(T/T_0)F_0$. Note that in both Eqs. (6) and (7) the void fraction ε cancels out.

On passing through the oxide bed, the gas phase is considered to retain thermodynamic equilibrium with the oxide. The ^{18}O-containing gas phase pulse passes through a 'sea of ^{16}O' captured by the oxide powder bed, ensuring, along with fast lattice diffusion of oxygen, that ^{16}O is returned to the gas phase upon every successful exchange event. In accord with Eq.(3), the main parameters thus governing surface exchange are the kinetic parameter $\Re_0$, which expresses the balanced exchange rate under equilibrium conditions, the available surface area $S_{\rm r}$ (hence, the amount of oxide powder or length of the packed bed), and the residence time of the reactor, $\tau_{\rm r}$. Reactor design and experimental conditions are chosen such that channeling, interphase and intraparticle diffusion are considered to be of minor importance and therefore can be neglected. This is further elaborated in this work.

B. Two-step oxygen exchange mechanism

The surface exchange rate, $\Re_0$, extracted from measurement merely is a lumped parameter, and may involve a sequence of possible reaction steps, each of which may be rate determining. Steps commonly considered include adsorption, dissociation, charge transfer, incorporation of oxygen into the oxide lattice, with possible intermediates like O_2^-, O_2^{2-} and O^-, of which only the superoxide ion, O_2^-, is known to be stable with respect to gaseous O_2 [33]. The altered distribution of isotopologues $^{18}O_2$, $^{16}O^{18}O$ and $^{16}O_2$ in the gas phase pulse, as occurring during passage through the reactor due to isotopic exchange/scrambling reactions at the oxide surface, holds important kinetic information about the exchange mechanism, as illustrated in FIG. 3.

The reversible oxygen exchange reaction may proceed via a consecutive two-step mechanism, as proposed ear-

DOI:10.1063/1674-0068/cjcp1811245

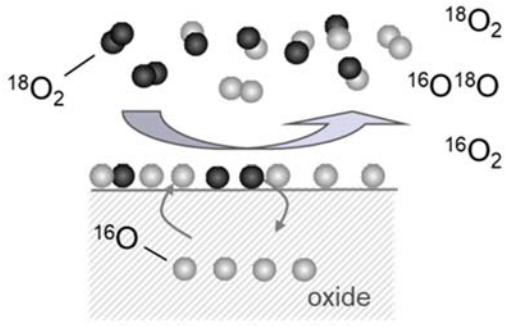

FIG. 3 Two-step oxygen exchange mechanism for the oxygen exchange reaction, with formation of mononuclear (i.e., dissociatively adsorbed) oxygen on the oxide surface as intermediate.

lier by Boukamp *et al.* [21]:

$$\text{Step 1} \qquad O_2^* \underset{\bar{\Re}_a}{\overset{\Re_a}{\longleftrightarrow}} 2O_{ad}^*$$

$$\text{Step 2} \qquad O_{ad}^* \underset{\bar{\Re}_i}{\overset{\Re_i}{\longleftrightarrow}} O_{lattice}$$

Each of the two steps, however, may still represent a grouping of specific elementary steps. Relevant for the interpretation of experimental data of isotopic exchange is that isotopic randomization is assumed to take place only after the dissociative adsorption step of oxygen at the surface (1st step). During its residence time at the surface, the oxygen adatom may combine either with another adatom and return to the gas phase as an O_2 molecule, or become exchanged with lattice oxygen (2nd step) before returning to the gas phase. Assuming low coverage of oxygen adatoms on the surface, it is easily shown that the overall rate of surface exchange rate can be expressed as

$$\Re_0 = \frac{\Re_i \Re_a}{\Re_a + \Re_i} \tag{8}$$

where $\Re_a$ is the rate of homolytic dissociative adsorption of O_2 molecules at the oxide surface, and $\Re_i$ is that of subsequent incorporation of the formed oxygen adatoms into the oxide lattice. In deriving Eq.(8), the occurrence of alternative pathways for oxygen exchange has been excluded, such as (i) the mutual exchange of oxygen between O_2 molecules in the gas phase, and (ii) possible swapping out of one of the oxygen atoms of the O_2 molecule for another oxygen during hypothetical formation of a three-atom complex between a gas phase O_2 molecule and an O adatom, or any other multi-atom complex between O_2 molecules and adsorbed species. In deriving the distribution of oxygen isotopologues $^{18}O_2$, $^{16}O^{18}O$ and $^{16}O_2$ in the effluent gas phase pulse, the more general treatment given earlier by Den Otter [15] is followed. Recognizing that

$$p = \frac{\Re_i}{\Re_a + \Re_i} \tag{9}$$

p represents the probability for successful exchange between oxygen residing on the surface and lattice oxygen, the time dependence of the gas phase fraction for $^{18}O_2$ can be expressed by the differential equation

$$n_r \frac{\partial f_g^{36}}{\partial t} = S\Re_a \left\{ -f_g^{36} + \left[f_g^{18} (1-p) \right]^2 \right\} \tag{10}$$

Eq.(10) is based on step 1 of two-step oxygen exchange mechanism, which is shown in FIG. 3. When $^{18}O_2$ is adsorbed on the surface of oxide, dissociated into ^{18}O atoms. Some of dissociated ^{18}O atoms successfully exchange with lattice oxygen ^{16}O, *i.e.*, $p \times f_g^{18}$, then the ^{16}O atoms on the surface form $^{16}O^{18}O$ and $^{16}O_2$. The rest of dissociated ^{18}O atoms combine to $^{18}O_2$, then $^{18}O_2$ molecules enter into the gas phase again with a probability of $f_g^{18}(1-p) \times f_g^{18}(1-p)$.

Substitution of Eq.(3) in Eq.(10), followed by integration over the time of residence in the reactor, τ_r, yields

$$\begin{aligned} f_{g,o}^{36} = {} & \frac{(1-p)^2}{1-2p} \left(f_{g,i}^{18} \right)^2 \exp\left(-\frac{2\Re_0 S \tau_r}{n_r} \right) + \\ & f_{g,i}^{36} \exp\left(-\frac{\Re_0 S \tau_r}{p n_r} \right) - \\ & \frac{(1-p)^2}{1-2p} \left(f_{g,i}^{18} \right)^2 \exp\left(-\frac{\Re_0 S \tau_r}{p n_r} \right) \end{aligned} \tag{11}$$

where $f_{g,i}^{36}$ and $f_{g,o}^{36}$ denote the $^{18}O_2$ fractions in the gas phase pulse at the inlet and outlet of the reactor, respectively. The corresponding $^{16}O^{18}O$ and $^{16}O_2$ fractions can be calculated from the conservation equations

$$f_g^{34} = 2\left(f_g^{18} - f_g^{36} \right) \tag{12}$$

$$f_g^{32} = 1 - f_g^{34} - f_g^{36} \tag{13}$$

which are valid at all coordinates in the reactor, ignoring axial dispersion in the plug flow reactor. In the theory developed by Klier *et al.* [17, 34], and independently by Boreskov and Muzykantov [13, 35], oxygen isotopic exchange is described to occur via three parallel one-step mechanisms: the O_2 molecule may exchange either one or both atoms with lattice oxygen (hetero exchange), at rates R_1 and R_2, respectively, or, without the involvement of lattice oxygen, *i.e*, only with oxygen from the gas phase (homo exchange), at a rate R_0. As discussed previously [15], if no other pathways for oxygen exchange are vivid, these three rates are constrained in the above 2-step model as: $R_1 = 2\sqrt{R_0 R_2}$.

III. EXPERIMENT

$(Y_2O_3)_{0.08}$-$(ZrO_2)_{0.92}$ (YSZ) powder (TOSOH, Japan, purity 99.9%) was calcined in air at 900 °C for 10 h. BSCF powder was prepared by solvent evaporation, and subsequent thermal decomposition

DOI:10.1063/1674-0068/cjcp1811245

of the precursor complexes, of an aqueous solution of metal nitrates in appropriate stoichiometry and to which ethylenediaminetetraacetic (EDTA) was added as complexing agent. The powder obtained was calcined in air at 800 °C for 24 h, and subsequently ball-milled in ethanol for 5 h. The milled powder was pressed into a disk via cold isostatic pressing at 4000 bar, and then sintered in air at 1100 °C for 10 h. The sintered disk was crushed to powder. The fraction of the powder passing a 120 mesh metal sieve was calcined in air at 950 °C for 10 h, and sieved again to remove possibly formed agglomerates. Heating and cooling rates in all cases were 3 °C/min. $La_2NiO_{4+\delta}$ powder was prepared similarly to BSCF, except that (i) the raw powder was calcined in air at 1000 °C for 10 h, (ii) the disk was sintered in air at 1370 °C for 10 h, and (iii) the crushed powder was calcined in air at 1100 °C for 10 h. The powders were characterized by X-ray powder diffraction (Philips XRD pananalitical PW1830), Brunauer-Emmet-Teller BET surface area (Micromeritics ASAP 2020M), and particle size (Mastersizer 2000, Malvern) measurements. The particle sizes were in the range of 2−5 μm, with BET surfaces of 10.12, 0.210, and 0.156 m^2/g for YSZ, BSCF and $La_2NiO_{4+\delta}$ respectively. X-ray diffraction confirmed that in all cases the desired structures were formed. Within the detection limit of XRD, no evidence was found for second phase formation or presence of other phase impurities.

PIE measurements were performed in the temperature range 350−900 °C with 25 °C intervals, at pO_2=0.21 atm, using a continuous flow packed-bed micro-reactor. The oxide powder was loaded between two quartz wool plugs in the center of the quartz tubular micro-reactor, having an inner diameter of 2 mm. The packed-bed length was typically in the range 12−20 mm. Two quartz rods with diameter ∼1 mm were used to minimize the free volume of the reactor. $^{16}O_2$ balanced with He to a $p(O_2)$ of 0.21 atm was used as carrier gas. The flow rate was 50 mL(NTP)/min, if not specified otherwise. Prior to measurements, the packed-bed micro-reactor was pre-treated at 850 °C for 2 h under a continuous flow of the carrier gas in order to remove possibly adsorbed water and CO_2, and subsequently cooled to room temperature, using heating/cooling rates of 3 °C/min. The response to an $^{18}O_2/N_2$ gas phase pulse (500 μL), with similar $p(O_2)$ as the carrier gas, passing through the reactor, was analyzed by online mass spectrometry (Omni Star^{TM} GSD 301 Pfeiffer-Vacuum). Oxygen isotope gas (>99 atom% $^{18}O_2$) was purchased from ISOTEC, Sigma-Aldrich. Nitrogen used as diluent for $^{18}O_2$ was also used for internal calibration of the mass spectrometer. A six-port valve with sample loop was used for injection of the pulse into the main carrier gas flow. The reactor was equilibrated for 15 min under continuous flow of the carrier gas prior to pulse injection. Measurements were conducted as a function of temperature, from room temperature onwards, by determining the $^{18}O_2$ and $^{16}O^{18}O$ concentrations in the effluent pulse. The integrated peak area of the oxygen isotope fraction of $^{16}O^{18}O$ was corrected for tailing, if present, by linear interpolation of the background. Average values of three pulse experiments at given temperature were used for calculations of the exchange rates. The mean residence time of the reactor varied between 5 and 40 ms, depending on the volumetric flow rate of the carrier gas at the temperature of the measurement, and the packed bed length. Additional measurements were carried out to check the presence of interphase (external) concentration gradients by varying the volumetric flow rate (25−100 mL(NTP)/min), and in case of YSZ, the packed bed length (6−27 mm). Experimental data obtained from heating and cooling runs agreed within experimental error.

IV. RESULTS AND DISCUSSION

A. PIE measurements

Mass spectroscopic data for $^{18}O_2$ and $^{16}O^{18}O$ obtained from PIE measurements on YSZ, BSCF and $La_2NiO_{4+\delta}$ as a function of temperature are shown in FIG. 4. Here, the appearance of $^{34}O_2$ pulse indicates that the ^{18}O atoms enter the oxides, which will slightly increase f_o^{18} in the oxide. However, even though all the ^{18}O atoms in the gas phase exchange with the ^{16}O atoms in the oxide, the average of f_o^{18} in the oxide is less than 0.2% in the all the experiments by assuming a fast lattice diffusion of oxygen in the oxide. On the other hand, f_g^{18} at the outlet of the reactor is more than 4% in all the experiments. Thus, f_g^{18} can be reasonably neglected in Eq.(2).

Corresponding isotope fractions $f_{g,o}^{36}$ and $f_{g,o}^{34}$ calculated from the integrated peak areas are shown in FIG. 5. $f_{g,o}^{32}$ was calculated using Eq.(13). Under the conditions of the experiments, the uptake of ^{18}O by the oxide becomes pronounced at elevated temperature. The corresponding onset temperatures are, however, different for the three compositions studied. This is, besides comparatively small differences in available surface area for exchange, mainly accounted for by the different specific activities for exchange exhibited by the materials. As seen from both FIG. 4 and FIG. 5, above the onset temperature of surface exchange, the $^{18}O_2$ signal and, hence, the corresponding isotope fraction, $f_{g,o}^{36}$, are found to decrease gradually with increasing temperature. This brings about associated changes in the isotope fractions of $^{16}O_2$ ($f_{g,o}^{32}$) and $^{16}O^{18}O$ ($f_{g,o}^{34}$) with increasing temperature. The latter behavior, found to be different for the three compositions, can be regarded as a fingerprint for the mechanism of surface oxygen exchange, *i.e.*, the rate of oxygen dissociative adsorption relative to that of oxygen incorporation, as discussed in more detail below.

As seen from FIG. 4, tailing of the $^{16}O^{18}O$ peak oc-

DOI:10.1063/1674-0068/cjcp1811245

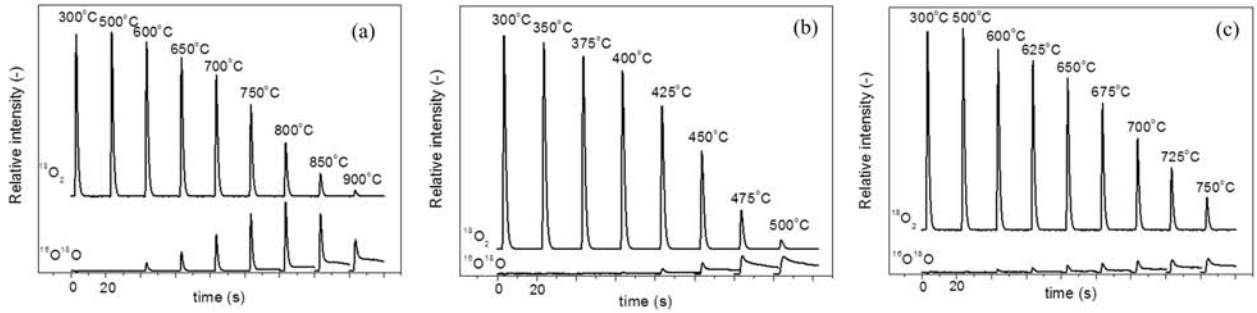

FIG. 4 Mass spectroscopic peaks for $^{18}O_2$ (m/z=36) and $^{16}O^{18}O$ (m/z=34) from PIE measurements as a function of temperature, for (a) YSZ, (b) BSCF, and (c) $La_2NiO_{4+\delta}$. Peaks obtained at different temperatures are shifted with respect to each other for reasons of clarity. Note that peak tailing is observed at the highest temperatures, and is only manifest for the $^{16}O^{18}O$ peak.

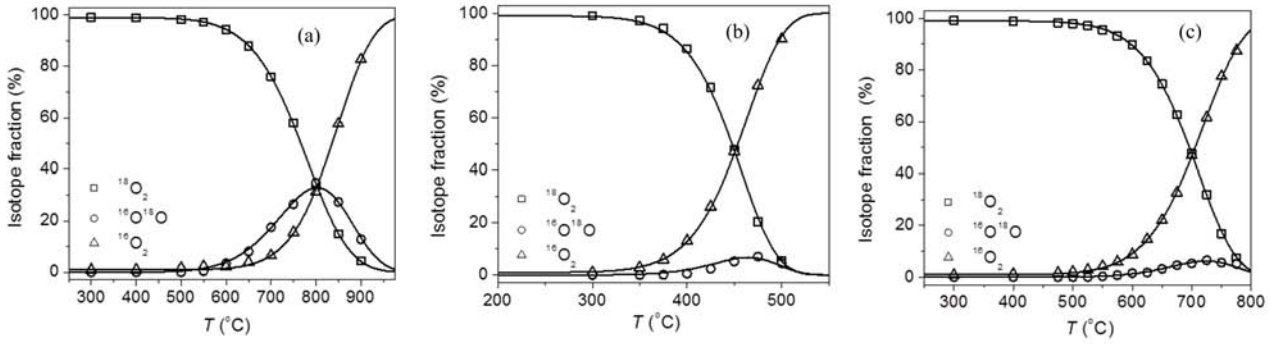

FIG. 5 Oxygen isotope fractions ($^{18}O_2$, $^{16}O^{18}O$ and $^{16}O_2$) as a function of temperature from PIE measurements on (a) YSZ, (b) BSCF, and (c) $La_2NiO_{4+\delta}$. Full lines are from model calculations, assuming constant activation energies for the rates of O_2 dissociative adsorption ($\Re_a$) and incorporation of oxygen adatoms into the oxide lattice ($\Re_i$). Maximum error bars are smaller than the size of the symbols.

curs at the highest temperature in the experiments. This observation is closely linked to the operating principle of the PIE technique, which essentially exploits the temporary hold-up of the ^{18}O isotope by (partial) incorporation into the oxide. The solid oxide forms a large reservoir of ^{16}O oxygen atoms. Hence, every successful exchange event implies a single transfer of ^{16}O to the gas phase, either in the form of $^{16}O^{18}O$ or $^{16}O_2$, depending on the relative rates of oxygen dissociative adsorption and oxygen incorporation, in conjunction with the extent of depletion of ^{18}O from the gas phase. Once the pulse has passed through the reactor, the (remaining) exchanged ^{18}O will be released from the oxide, with an approximate release time constant $\tau_{release}=m_r/\Re_0 S$, where m_r is the total number of oxide lattice oxygen in the reactor volume. The latter time constant should be compared with that of ^{18}O uptake during passage of the pulse, $\tau_{uptake}=n_r/\Re_0 S$, where n_r is the total number of gas phase oxygen atoms in the reactor volume (c.f. Eq.(2)). Since $m_r \gg n_r$, it is obvious that $\tau_{release} \gg \tau_{uptake}$. At high temperatures, where oxygen exchange is comparatively fast, $\tau_{release}$ approaching the time scale of the pulse experiment, the release of ^{18}O from the oxide may induce peak tailing. Since the concentration of ^{18}O atoms in the oxide is small, their recombination to O_2 molecules occurs predominantly with excess ^{16}O. Significant peak tailing therefore might be manifest only for the $^{16}O^{18}O$ peak. Since a master equation for peak tailing was lacking, integrated $^{16}O^{18}O$ peak areas were corrected for tailing, if present, by a simple linear interpolation of the background. For calculation of the ^{18}O uptake by the oxide and, hence, the effective surface exchange rate, the peak tailing correction of the $^{16}O^{18}O$ peak at high temperature was usually found to be marginal relative to the concomitant decrease of the $^{18}O_2$ peak as a result of oxygen exchange.

B. Oxygen surface exchange rate

FIG. 6 shows Arrhenius plots of the overall surface exchange rate, $\Re_0$, for the three compositions calculated using Eq.(4). The results confirm that BSCF exhibits comparatively high exchange rates, whose values are among the highest reported in literature [36]. The exchange rate of BSCF, at 500 °C, is found to be almost 4 orders of magnitude higher than that of YSZ. Activation energies for $\Re_0$ extracted from the Arrhenius plots

DOI:10.1063/1674-0068/cjcp1811245

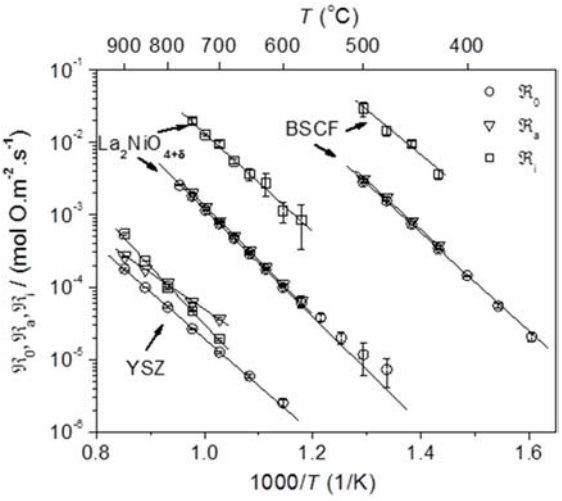

FIG. 6 Temperature dependence of the rate of oxygen exchange ($\Re_0$), oxygen dissociative adsorption ($\Re_a$), and oxygen incorporation ($\Re_i$) for YSZ, BSCF, and $La_2NiO_{4+\delta}$. The error bars show the maximum errors.

TABLE I Apparent activation energies of $\Re_0$, $\Re_a$, and $\Re_i$ from PIE measurements.

Oxide	$\Re_0$/(kJ/mol)	$\Re_a$/(kJ/mol)	$\Re_i$/(kJ/mol)
YSZ	121.4±1.3	95.6±2.9	156.3±6.0
BSCF	132.1±1.2	128.1±3.5	120.5±12.0
$La_2NiO_{4+\delta}$	130.3±2.1	140.4±1.2	132.0±5.2

are listed in Table I.

For each of the compositions studied, the exchange rates are found to be in good agreement with data from previous studies, measured using either electrical conductivity relaxation and/or the isotopic exchange depth profiling (IEDP) technique [36−40].

Data obtained from different studies are compared in FIGs. 7, 8 and 9 for YSZ, BSCF and $La_2NiO_{4+\delta}$, respectively. To enable comparison, the surface exchange rate, $\Re_0$ was recalculated to the surface exchange coefficient k^* using $k^*=\Re_0/C_O$, where C_O is the concentration of oxygen in the oxide. Discrepancies between the values obtained in different studies for each of the compositions can be, at least partly, accounted for by differences in the experimental conditions, pre-annealing procedures, and morphology of the samples (*e.g.* single crystal versus polycrystalline samples).

C. Two-step oxygen exchange mechanism

As discussed in the above section, the observed distribution of $^{18}O_2$, $^{16}O^{18}O$ and $^{16}O_2$ isotopologues in the effluent pulse allows one to deconvolute the overall exchange rate, $\Re_0$, into $\Re_a$ and $\Re_i$, representing the apparent rate of O_2 dissociative adsorption and that of the subsequent incorporation of oxygen adatoms into the

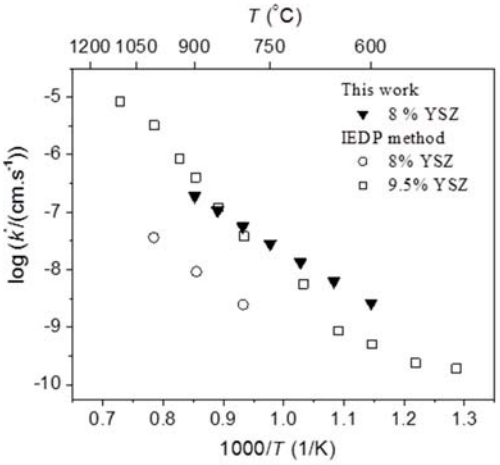

FIG. 7 Comparison of k^* of YSZ measured by this work (pO_2=0.21 atm) and by IEDP method ($p(O_2)$=1 atm): 8% YSZ in Ref.[37] and 9.5% YSZ in Ref.[40].

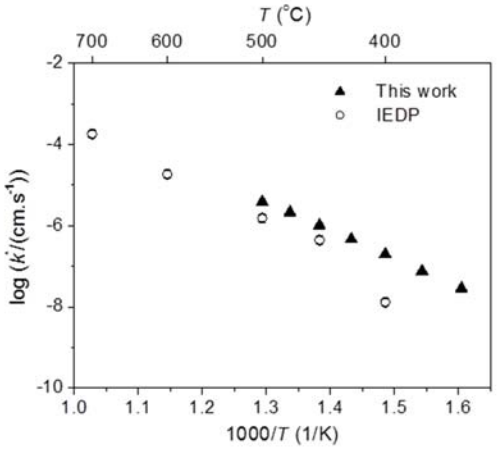

FIG. 8 Comparison of k^* of BSCF measured by this work ($p(O_2)$=0.21 atm) and by IEDP method ($p(O_2)$=0.5 atm) in Ref.[36].

oxide lattice, respectively. Results of such calculations, using Eqs.(8−11), are displayed in FIG. 6. Apparent activation energies and pre-exponential factors of $\Re_a$ and $\Re_i$ for the different materials are listed in Table I. These were assumed to be constant within the investigated temperature range and used in re-calculation of the isotope fractions $f^{36}_{g,o}$, $f^{34}_{g,o}$, and $f^{32}_{g,o}$ in the effluent pulse as a function of temperature, as displayed (full lines) in FIG. 5.

Under the conditions of the experiments, oxygen surface exchange on both mixed ionic-electronic conductors $La_2NiO_{4+\delta}$ and BSCF appears to be limited by the apparent rate of O_2 dissociative adsorption. As can be seen from FIG. 6, for both materials $\Re_i$ is almost one order of magnitude higher than $\Re_a$. More systematic studies are needed to clarify which elementary step controls the lumped reaction rate, $\Re_a$ (for example, chemisorption). The results line up with observations

DOI:10.1063/1674-0068/cjcp1811245

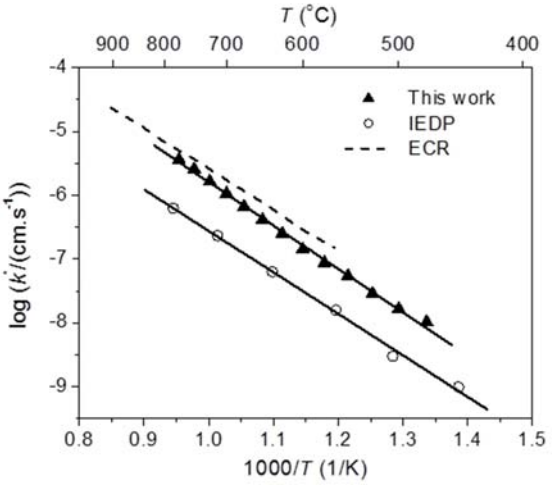

FIG. 9 Comparison of k^* of $La_2NiO_{4+\delta}$ measured by this work and by IEDP in Ref.[38] and ECR methods in Ref.[39], all at $p(O_2)$=0.21 atm.

made for other oxide ion conducting solids, including the fluorite-structured 25 mol% erbia-stabilized Bi_2O_3 [14, 21]. In the cited studies, data of oxygen isotopic exchange were obtained using the IEGE technique and analyzed using the current two-step exchange model. For the solid electrolyte YSZ investigated in the current study, the rates of O_2 dissociative adsorption and oxygen incorporation reactions are found to compete with each other in the range of temperatures investigated. For this material, an apparent change-over takes place from exchange limited by the rate of oxygen incorporation below ∼800 °C to exchange limited by the rate of O_2 dissociative adsorption above this temperature.

D. Reactor analysis

Within the range of temperatures studied, blank experiments carried out at a carrier gas flow rate of 50 mL(NTP)/min revealed no significant exchange activity of the empty quartz micro-reactor, shown in FIG. 10. Note that some isotope fractionation only occurs at the highest temperature and lowest flow rate (F=25 mL/min), indicating some gas mixing of the pulse with the carrier gas (due to axial dispersion) and catalytic activity of the empty quartz reactor.

A series of semi-empirical relations to assure that the reactor operates under plug flow conditions are discussed below. The analysis is mainly based on recommendations and criteria as, for example, reviewed by Perez-Ramirez *et al.* [41] and Mederos *et al.* [42].

1. Minimum reactor diameter

Wall flow leads to enhanced axial dispersion because of a higher flow in regions near the wall where the packing void fraction is higher. A criterion to neglect wall effects in fixed-bed reactors is [41]

$$\frac{d_r}{d_p} > 10 \tag{14}$$

where d_r and d_p are the reactor and particle diameters, respectively.

2. Minimum packed-bed length

Axial mass dispersion is always present, but can be minimized by selecting a proper value of the bed length, L_{pb}, to particle diameter, d_p, ratio [41]

$$\frac{L_{pb}}{d_p} > \frac{20n}{Pe} \ln\left(\frac{1}{1-x}\right) \tag{15}$$

where n denotes the reaction order, x is the fractional conversion, and Pe is the Péclet particle number. A first order rate law for isotopic exchange is in accord with McKay's law [17, 20]. For operation in laboratory scale reactors (*i.e.*, at low Reynold numbers), a value of Pe≈0.5 is commonly used to check the criterion [43]. A rule of thumb for criterion is [41]

$$\frac{L_{pb}}{d_p} > 50 \tag{16}$$

3. Interphase (external or extraparticle) mass transfer

To minimize concentration gradients between the external surface of oxide particles and adjacent bulk gas regions, the following criterion must be fulfilled for an isothermal nth order irreversible reaction [41]

$$Ca = \frac{0.5\,\Re_{vol}}{S_p k_{O_2} C_b} < \frac{0.05}{|n|} \tag{17}$$

where Ca denotes the dimensionless Carberry number, $\Re_{vol}$ is the exchange rate per unit particle volume, S_p is the specific surface area of the particle, k_{O_2} is the mass transfer coefficient, and C_b is the concentration of oxygen in the bulk gas, respectively. The presence of interphase concentration gradients can be recognized when the apparent exchange rate is a function of the reactant flow rate. Moreover, if the apparent activation energy is less than 20 kJ/mol, interphase diffusion limitations are highly suspected [44].

4. Intraparticle (internal) mass transfer

Internal concentration gradients may arise in pores of individual oxide particles. These are excluded in the present study by measuring on oxide powders obtained by crushing dense ceramics.

DOI:10.1063/1674-0068/cjcp1811245

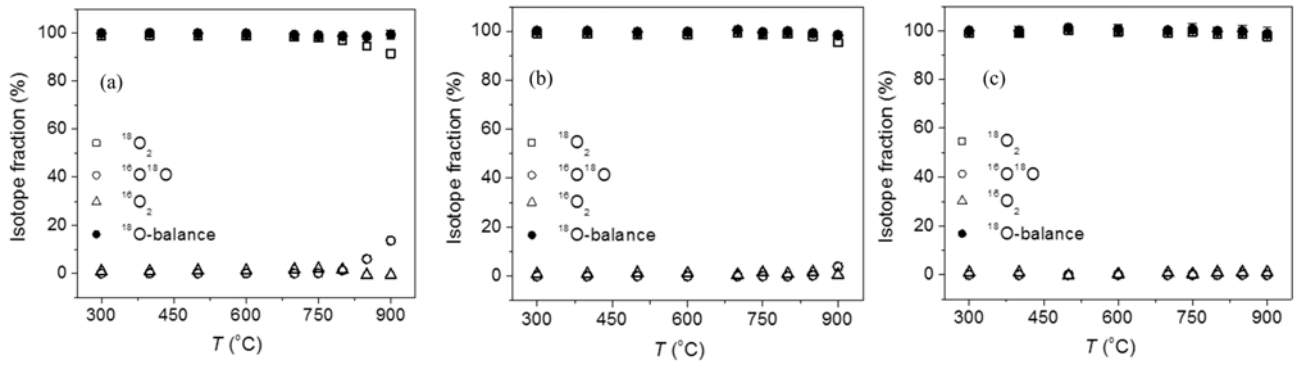

FIG. 10 Oxygen isotope fractions ($^{18}O_2$, $^{16}O^{18}O$, and $^{16}O_2$) in the effluent pulse and ^{18}O-balance as a function of temperature from PIE measurements for an empty reactor carried out at different carrier gas flow rates (a) F=25 mL/min, (b) F=50 mL/min, and (c) F=100 mL/min.

5. Pressure drop across the packed bed

The axial pressure drop across the entire bed can be calculated using the Ergun equation [45]

$$\Delta P_{\rm b} = L_{\rm pb}\left[\frac{150\,\mu_{\rm g}}{{d_{\rm p}}^2}\frac{(1-\varepsilon)^2}{\varepsilon^3}u + \frac{1.75\,\rho_{\rm g}}{d_{\rm p}}\frac{(1-\varepsilon)}{\varepsilon^3}u^2\right] \quad (18)$$

where $\mu_{\rm g}$ is the (dynamic) gas viscosity, ε is the void fraction of the bed, u is the superficial velocity, and $\rho_{\rm g}$ is the gas density. A rule of thumb is that the pressure drop should be lower than ∼20%. If the particle size $d_{\rm p}$ is too small, a significant pressure is obtained. In this case the problem may be resolved by mixing the oxide particles with inert particles with larger size [46].

To exemplify the validity of the different criteria in PIE measurements, calculations were performed using experimental conditions and data for $La_2NiO_{4+\delta}$. Results of these calculations are given in Table II.

The experimental values for $L_{\rm pb}$=15 mm, $d_{\rm p}$=28.9 μm, $d_{\rm r}$=2 mm yield $L_{\rm pb}/d_{\rm p}$=519 and $d_{\rm r}/d_{\rm p}$=69.2, where ratios comply with the requirements for a minimum reactor diameter and minimum bed length. The calculated Carberry numbers are very small (mainly due to the small particle size), and indicate the absence of interphase concentration gradients up to a high conversion (x), which corresponds to a high level of depletion of ^{18}O from the gas phase. The calculations further demonstrate that in this case the use of larger particles could have been considered to overcome the pressure drop problem at high temperatures.

To prevent intraparticle concentration gradients, possibly developing in micro- or mesopores of the oxide, the exchange measurements were conducted on powders obtained by crushing sintered ceramics. To check for the presence of interphase (external) concentration gradients, additional measurements were conducted at 25 and 100 mL(NTP)/min, besides at 50 mL(NTP)/min, the results are shown in FIG. 11. The good agreement noted between the exchange rates obtained at different flow rates suggests the absence of significant interphase concentration gradients in the experiments. In addition, in the case of YSZ, the length of the packed bed varies in the range of 6.3−26.4 mm, shown in FIG. 12, and the results verify the absence of significant interphase concentration gradients. In neither experiment evidence could be found for interphase concentration gradients. The exchange rates obtained from the different experiments carried out for each composition are found to agree within experimental error. It should be noted that the apparent activation energies as listed in Table II also do not suggest the presence of significant interphase concentration gradients. Only if the apparent activation energy is less than 20 kJ/mol, interphase diffusion limitations might be suspected [44].

TABLE II Evaluation of selected plug flow criteria (see text).

T/°C	x	$\frac{20\,n}{Pe}\ln\left(\frac{1}{1-x}\right)$	Ca	$\Delta p_{\rm b}$/atm
500	1.1%	0.4	1.1×10^{-6}	0.14
550	3.4%	1.4	3.5×10^{-6}	0.16
600	8.6%	3.6	8.8×10^{-6}	0.17
650	23.0%	10.4	2.5×10^{-5}	0.19
700	49.1%	27.0	6.2×10^{-5}	0.21
750	80.2%	64.7	1.4×10^{-4}	0.23

V. CONCLUSION

In summary, we have developed a highly versatile technique for measuring the rate of oxygen surface exchange on solid oxide ion conductors. The developed PIE technique is rapid, simple, and highly suitable for screening studies to identify candidate materials for potential applications, which rely on oxide materials exhibiting fast surface exchange kinetics (such as solid oxide fuel cells and oxygen transport membranes). The

DOI:10.1063/1674-0068/cjcp1811245

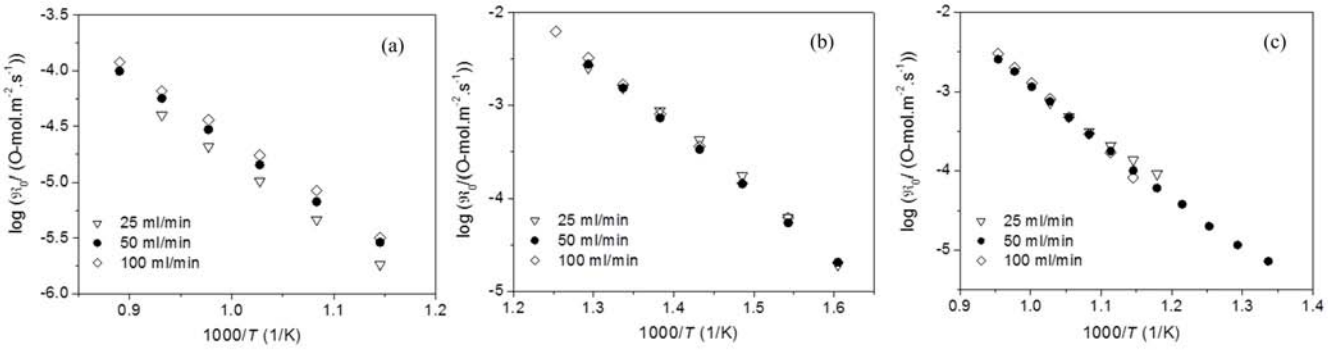

FIG. 11 Oxygen exchange rate ($\Re_0$) as a function of inverse temperature assessed from PIE measurements carried out at different carrier gas flow rates, for (a) YSZ, (b) BSCF, and (c) $La_2NiO_{4+\delta}$.

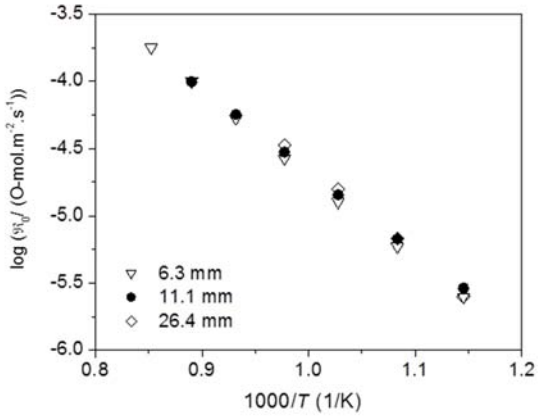

FIG. 12 Oxygen exchange rate ($\Re_0$) of YSZ as a function of inverse temperature assessed from PIE measurements carried out at different packed-bed lengths.

technique can be used in systematic studies towards factors governing oxygen surface exchange. Possible factors include the partial ionic and electronic conductivities, oxygen nonstoichiometry, catalytic properties of the constituent ions, *etc.* The PIE technique is further amenable to *in situ* analysis of the effect of environmental conditions (temperature and oxygen partial pressure) and gas phase impurities, *e.g.*, H_2O and CO_2, on oxygen surface exchange. No rapid heating/quenching steps are required to facilitate ^{18}O tracer anneal or analysis, as for example in commonly used IEDP and IEGE techniques, while data collection and analysis in the application of PIE are simple and straightforward. Direct measurement of the $^{18}O_2$, $^{16}O^{18}O$, and $^{16}O_2$ isotope fractions in the effluent pulse, *i.e.*, after passing through a continuous flow packed-bed micro-reactor loaded with the oxide powder, by on-line mass spectrometry at the exit of the reactor, enables evaluation of the exchange rate from the net uptake of ^{18}O by the sample, the residence time and surface area available for exchange. The relative distribution of the oxygen isotopologues in the effluent pulse provides insight into the mechanism of the oxygen exchange reaction.

In the current work, the PIE technique has been demonstrated by measuring the exchange rate of selected well-known oxides showing enhanced oxide ionic conductivity, including YSZ, BSCF, and $La_2NiO_{4+\delta}$. Measurements were performed, at $p(O_2)$=0.21 atm, in the temperature range of 350−900 °C. The results confirm that BSCF exhibits comparatively high exchange rates, which are among the highest values reported in literature. Comparison is made with experimental data from previous studies measured by electrical conductivity relaxation and isotopic exchange depth profiling methods. For all three materials good agreement is obtained with published data. Analysis of the data from PIE in terms of a model with two consecutive, lumped steps for the exchange reaction shows that the exchange rate exhibited by the mixed conductors $La_2NiO_{4+\delta}$ and BSCF is limited by the apparent rate of dissociative adsorption of O_2 molecules at the oxide surface. For the solid electrolyte YSZ a change-over takes place, from rate-limitations by oxygen incorporation below ∼800 °C to rate-limitations by O_2 dissociative adsorption above this temperature. More systematic studies are needed to clarify the elementary reaction(s) controlling both lumped reaction steps in the adopted two-step model.

VI. ACKNOWLEDGMENTS

Prof. dr. ir. H. J. M. Bouwmeester (University of Twente, The Netherlands) is acknowledged for fruitful discussions and suggestions.

[1] B. A. Boukamp, Nat. Mater. **2**, 294 (2003).
[2] C. S. Chen, S. J. Feng, S. Ran, D. C. Zhu, W. Liu, and H. J. M. Bouwmeester, Angew. Chem. Int. Edit. **42**, 5196 (2003).
[3] S. Karazhanov and V. Kharton, Mater. Lett. **229**, 5 (2018).
[4] Z. P. Shao and S. M. Haile, Nature **431**, 170 (2004).

DOI:10.1063/1674-0068/cjcp1811245

[5] C. L. Song and S. M. Fang, Chin. J. Chem. Phys. **27**, 445 (2014).
[6] J. R. Wilson, W. Kobsiriphat, R. Mendoza, H. Y. Chen, J. M. Hiller, D. J. Miller, K. Thornton, P. W. Voorhees, S. B. Adler, and S. A. Barnett, Nat. Mater. **5**, 541 (2006).
[7] R. Q. Yan, W. Liu, and C. L. Song, Chin. J. Chem. Phys. **27**, 690 (2014).
[8] E. Boehm, J. M. Bassat, M. C. Steil, P. Dordor, F. Mauvy, and J. C. Grenier, Solid State Sci. **5**, 973 (2003).
[9] J. A. Lane and J. A. Kilner, Solid State Ionics **136**, 997 (2000).
[10] B. Ma, U. Balachandran, J. H. Park, and C. U. Segre, Solid State Ionics **83**, 65 (1996).
[11] J. E. tenElshof, M. H. R. Lankhorst, and H. J. M. Bouwmeester, J. Electrochem. Soc. **144**, 1060 (1997).
[12] T. H. Lee, Y. L. Yang, A. J. Jacobson, B. Abeles, and M. Zhou, Solid State Ionics **100**, 77 (1997).
[13] G. K. Boreskov, Adv. Catal. **15**, 285 (1964).
[14] B. A. Boukamp, I. C. Vinke, K. J. Devries, and A. J. Burggraaf, Solid State Ionics **32-33**, 918 (1989).
[15] M. W. den Otter, B. A. Boukamp, and H. J. M. Bouwmeester, Solid State Ionics **139**, 89 (2001).
[16] J. A. Kilner, B. C. H. Steele, and L. Ilkov, Solid State Ionics **12**, 89 (1984).
[17] K. Klier, J. Novakova, and P. Jiru, J. Catal. **2**, 479 (1963).
[18] E. K. Kurumchin and M. V. Perfiliev, Solid State Ionics **42**, 129 (1990).
[19] J. Novakova, Catal. Rev. **4**, 77 (1970).
[20] D. S. Tannhauser, J. A. Kilner, and B. C. H. Steele, Nucl. Instrum. Methods Phys. Res. **218**, 504 (1983).
[21] B. A. Boukamp, B. A. Vanhassel, I. C. Vinke, K. J. Devries, and A. J. Burggraaf, Electrochim. Acta **38**, 1817 (1993).
[22] S. Diethelm, A. Closset, J. Van herle, and K. Nisancioglu, J. Electrochem. Soc. **149**, E424 (2002).
[23] S. F. Bychkov, I. I. Gainutdinov, S. A. Chizhik, and A. P. Nemudry, Solid State Ionics **320**, 297 (2018).
[24] H. J. M. Bouwmeester, C. L. Song, J. J. Zhu, J. X. Yi, M. V. Annaland, and B. A. Boukamp, Phys. Chem. Chem. Phys. **11**, 9640 (2009).
[25] M. Borysiuk, P. Kristiansson, N. Arteaga-Marrero, M. Elfman, P. Golubev, E. J. C. Nilsson, C. Nilsson, J. Pallon, and N. Salim, Nucl. Instrum. Methods Phys. Res. Sec. B **269**, 2229 (2011).
[26] S. Bedrane, C. Descorme, and D. Duprez, Appl. Catal. A: gen. **289**, 90 (2005).
[27] F. Dong, A. Suda, T. Tanabe, Y. Nagai, H. Sobukawa, H. Shinjoh, A. Sugiura, C. Descorme, and D. Duprez, Catal. Today **90**, 223 (2004).
[28] R. A. De Souza and R. J. Chater, Solid State Ionics **176**, 1915 (2005).
[29] P. Fielitz and G. Borchardt, Solid State Ionics **144**, 71 (2001).
[30] S. L. Shannon and J. G. Goodwin, Chem. Rev. **95**, 677 (1995).
[31] C. C. Kan, H. H. Kan, F. M. Van Assche, E. N. Armstrong, and E. D. Wachsman, J. Electrochem. Soc. **155**, B985 (2008).
[32] A. Bueno-Lopez, K. Krishna, and M. Makkee, Appl. Catal. A **342**, 144 (2008).
[33] S. B. Adler, X. Y. Chen, and J. R. Wilson, J. Catal. **245**, 91 (2007).
[34] K. Klier and E. Kucera, J. Phys. Chem. Solids **27**, 1087 (1966).
[35] V. S. Muzykantov, G. K. Boreskov, and G. I. Panov, React. Kinet. Catal. L **1**, 315 (1974).
[36] L. Wang, R. Merkle, J. Maier, T. Acarturk, and U. Starke, Appl. Phys. Lett. **94**, (2009).
[37] Y. Ji, J. A. Kilner, and M. F. Carolan, Solid State Ionics **176**, 937 (2005).
[38] J. A. Kilner and C. K. M. Shaw, Solid State Ionics **154**, 523 (2002).
[39] G. Kim, S. Wang, A. J. Jacobson, L. Reimus, P. Brodersen, and C. A. Mims, J. Mater. Chem. **17**, 2500 (2007).
[40] P. S. Manning, J. D. Sirman, R. A. DeSouza, and J. A. Kilner, Solid State Ionics **100**, 1 (1997).
[41] J. Perez-Ramirez, R. J. Berger, G. Mul, F. Kapteijn, and J. A. Moulijn, Catal. Today **60**, 93 (2000).
[42] F. S. Mederos, J. Ancheyta, and J. W. Chen, Appl. Catal. A **355**, 1 (2009).
[43] J. Perez-Ramirez, J. M. Garcia-Cortes, F. Kapteijn, G. Mul, J. A. Moulijn, and C. S. M. de Lecea, Appl. Catal. B **29**, 285 (2001).
[44] C. Perego and S. Peratello, Catal. Today **52**, 133 (1999).
[45] S. Ergun, Chem. Eng. Prog. **48**, 227 (1952).
[46] M. H. Aldahhan, Y. X. Wu, and M. P. Dudukovic, Ind. Eng. Chem. Res. **34**, 741 (1995).

DOI:10.1063/1674-0068/cjcp1811245